Asian Journal of Chemistry; Vol. 26, No. 18 (2014), 6050-6054

ASIAN JOURNAL OF CHEMISTRY

http://dx.doi.org/10.14233/ajchem.2014.16586

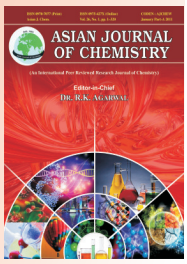

Effect of Temperature on Shape & Optical Properties of MgO/ZnO Nanocomposites

K. TAMIZH SELVI[1,*], M. RATHNAKUMARI[2], M. PRIYA[3] and P. SURESH KUMAR[2]

[1]Department of Physics, Vel Tech High Tech Engineering College, Avadi, Chennai-600 062, India
[2]Department of Physics, Velammal Engineering College, Chennai-600 066, India
[3]Department of Physics, Saveetha Engineering College, Chennai-602 105, India

*Corresponding author: E-mail: yadava_tamizhselvi@rediffmail.com

Received: 26 October 2013; *Accepted*: 22 February 2014; *Published online*: 1 September 2014; AJC-15852

MgO/ZnO nanocomposites were synthesized by mixing magnesium acetate tetrahydrate and zinc acetate in the equimolar ratio through a simple reflux method. The refluxed sample was annealed at three different temperatures 400, 500 and 600 ºC, respectively. X-ray diffraction spectra (XRD) showed wurtzite ZnO structure with cubic MgO. The HR-SEM picture showed the rod shaped morphology at 400 °C and morphology changed to spherical shape with the increase in temperature to 600 °C. Williamson-Hall plot is used to study the particle size and micro strain of the synthesized MgO/ZnO nanocomposites. The band gap and luminescent property were investigated using ultra violet-visible and photoluminescence spectra. The optical property of MgO/ZnO nanocomposites depends on the annealing temperature which is shown by the increase in the band gap as temperature increases.

Keywords: MgO-ZnO nanocomposites, Photoluminescence, Ultra violet-visible, HRSEM and EDAX.

INTRODUCTION

Synthesis of nanocomposites in nanofield has drawn much attention due to their potential applications in nanoscale electronics and opto-electronic devices. The properties of nanocomposite materials depend not only on the properties of their individual parents but also on their morphology and interfacial characteristics. Thus, nanocomposites promise new applications in many fields such as mechanically reinforced lightweight components, non-linear optics, battery cathodes, nanowires, sensors and other systems[1-4]. Metallic nanocomposites could offer distinct advantages over polymeric composites due to the inherent high temperature stability, high strength, high modulus, wear resistance and thermal and electrical conductivity of the metal matrix.

Magnesium oxide (MgO) nanoparticle is thermodynamically stable and wide band gap (7.2 eV) material. It has application as a protective layer in plasma display panel[5], paint, toxic waste water remediation, refractory materials, sensor and superconducting products[6-8]. Magnesium oxide is a best candidate for the barrier material in super sensitive low field sensor called Magnetic Tunnel Junction (MTJ) sensors, because of its superior Tunneling magneto-resistance (TMR) value compared to AlOx[9,10]. Zinc oxide is a wide bang gap (3.37 eV) semiconductor oxide and it is a promising material for electronic and opto electronic applications such as field emitters, ultraviolet lasers, photo catalysts[11], gas sensor[12-13] controlling units as UV photo detectors and as high-flame detectors[14].

Many researchers have investigated the combined effect of these MgO-ZnO nanocomposites for several applications[15-18]. These MgO-ZnO nanocomposites find its use as a polycarboxylate dental cement[18]. The photocatalytic activity of ZnO was enhanced by the addition of highly hygroscopic and nanoporous MgO[19].

In this research, we successfully synthesized the powder form of MgO-ZnO nanocomposites through a simple reflux method with different annealing temperatures. Their band gap and luminescent properties were investigated. The physical properties of synthesized powder sample were studied by using different characterization techniques such as XRD, HRSEM with EDAX, TG/DTA, UV and photoluminescent spectra.

EXPERIMENTAL

Analytical grade (AR) magnesium acetate tetrahydrate, zinc acetate is used as a starting material. AR grade ethanol is used as a solvent. Acetic acid is taken as a gelling agent.

Preparation of MgO-ZnO nanoparticles and nanorods: For the synthesis of MgO-ZnO nanoparticles, magnesium acetate tetrahydrate and zinc acetate is taken in equimolar ratio 1:1. Both precursors are dissolved separately with 50 mL ethanol and the magnesium acetate and zinc acetate solutions were mixed and stirred well to get a homogeneous solutions.

This solution was transferred into a round bottom flask and the solution was refluxed at a temperature of 90 °C for 1 h. The solid obtained was dried at 90 °C for 6 h and annealed at three temperatures 400 °C, 500 °C and 600 °C for 2 h. The annealed samples were labeled as sample-1 (400 °C), sample-2 (500 °C) and sample-3 (600 °C), respectively. The samples are characterized by X-ray diffractometer (XRD) with CuKα radiation in the range of 10-80° (λ = 0.154 nm). HRSEM is recorded using FEI Quanta FEG 200 high resolution scanning electron microscope. The thermal decomposition temperature is obtained by using TG/DTA. UV-visible absorption spectra of MgO/ZnO nanocomposites were recorded using a Varian Cary 5E spectrophotometer at room temperature in the range of 200-800 nm. The photoluminescence spectra of MgO/ZnO nanocomposite were recorded by the Perkin-Elmer lambda 900 spectrophotometer with a Xe lamp as the excitation light source.

RESULTS AND DISCUSSION

Fig. 1 shows the TG/DTA curve of as-synthesized powder sample. The peak at 101.75 °C corresponds to the sample removes all the volatile species (water, ethanol, acetic acid). The exothermic peaks within 250-400 °C, shows the sample removes the residual organic matter such as carboxylate species and hydroxyl groups. Above 400 °C, the mass loss was negligible. Based on this TGA trace, the as-synthesized sample were calcined at 400, 500 and 600 °C, respectively for 2 h.

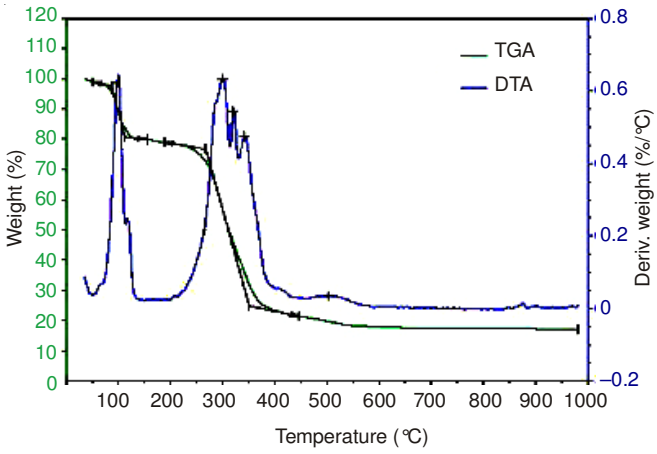

Fig. 1. TG/DTA curve as-synthesized powder sample

XRD analysis: Fig. 2 shows the XRD patterns of MgO-ZnO nanoparticles of different temperatures. All the samples exhibit major peaks at 31.878° (100)*, 34.608° (002)*, 36.318° (101)*, 47.705° (102)*, 56.675° (110)*, 63.138° (103)*, 66.34° (200)*, 68.076° (112)*, 69.107° (201)* are assigned to hexagonal wurtzite ZnO[20-21]. The other peaks at 42.909° (200), 62.242° (220), 74.59° (311) and 78.538° (222) are assigned to cubic MgO[22-23]. The asterisk (*) marked in Fig. 2 denotes the wurtzite ZnO phase. The XRD picture shows that the peak intensity increases with increasing temperature. It corresponds to the formation of different morphologies of MgO/ZnO nanocomposites. Usually, the basic parameter such as solvent, precursor concentration, calcining temperature, time, *etc*., influences the morphology and luminescence properties[24]. Therefore, the annealing temperature strongly influences the morphology of the MgO/ZnO nanoparticles.

We used the Williamson-Hall plot equation[25] to calculate particle size and Micro strain of the synthesized MgO-ZnO nanocomposites. Micro strain is due to the imperfections within the crystalline lattice, including vacancies, dislocations, stacking faults and others. A plot is drawn with 4 sinθ along the X-axis and B cosθ along the Y-axis for synthesized MgO-ZnO nanocomposites as shown in Fig. 3. From the linear fit to the data, the crystalline size was estimated from the *y*-intercept and the strain from the slope of the fit. The Williamson-Hall equation is,

$$B\cos\theta = \frac{k\lambda}{t} + 4\varepsilon\sin\theta \qquad (1)$$

where B is Full-width at half maxima, θ is the angle of diffraction, τ is the particle size calculated from X-ray diffraction spectra, ε is the micro-strain and λ is the wavelength of Cukα radiation [λ = 1.54056 Å]. The dislocation density is calculated using the relation $\delta = 1/D^2$ (lines/Sq. meter) where D is the particle size. The average crystallite size, micro-strain and dislocation density with different annealing temperature is listed in Table-1. As shown in Table-1, the less crystallite size is calculated for sample-3.

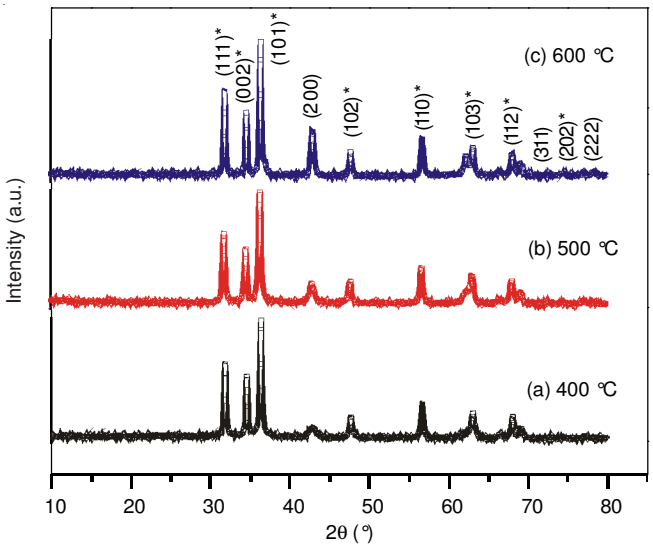

Fig. 2. XRD spectrum of MgO-ZnO nanoparticles (a) after calcination 400 °C and (b) after calcination 500 °C (c) after calcination 600 °C

TABLE-1
CRYSTALLITE SIZE, MICRO-STRAIN AND DISLOCATION DENSITY VARIATION WITH DIFFERENT ANNEALING TEMPERATURE

S. No.	Sample	Temperature and time	Particle size by W-H plot (nm)	Micro strain	Dislocation density (δ) (lines/Sq. meter)
1.	Sample-1	400 °C, 2h	25.2	0.000621	0.001575
2.	Sample-2	500 °C, 2h	29.6	0.00321	0.001141
3.	Sample-3	600 °C, 2h	23.4	0.00151	0.001826

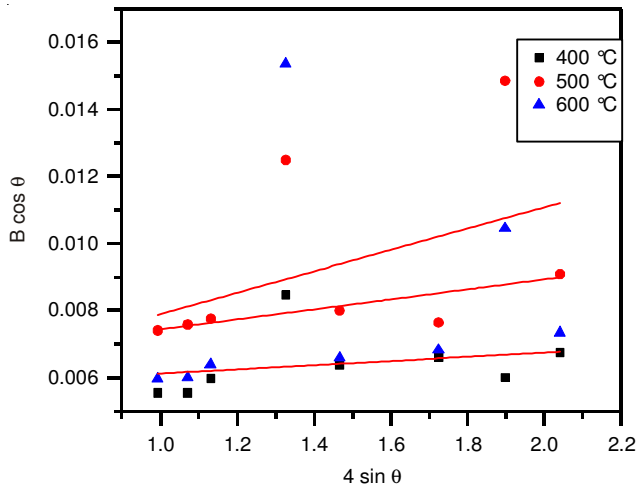

Fig. 3. Williamson-Hall plot for the MgO-ZnO nanopowder synthesized after the calcination of (a) 400 °C (b) 500 °C and (c) 600 °C

HRSEM and EDX analysis: Fig. 4 shows the HRSEM pictures of sample-1, sample-2 and sample-3, respectively. These pictures reveal that morphology strongly depends on the temperature. The images showed rod-like and spheroid morphologies. At 400 °C, MgO/ZnO nanocomposite forms the rod shape whose diameter is in the range of 30-40 nm shown in Fig. 4a, b. At 500 °C, the rod shape is prostrated, the length of the rod is reduced and it tries to take spherical shape shown in Fig. 4c, d). These shape transition completes at 600 °C. At 600 ºC the MgO/ZnO nanocomposites takes the complete spherical shape of less agglomeration shown in Fig. 4e, f.

Fig. 5 shows the EDX spectrum of sample-1, sample-2 and sample-3, respectively. The spectrum showed that the synthesized MgO/ZnO nanocomposite consists of only elements of Mg, Zn and O and their compositions are given in table (inset of EDX spectrum). This confirms the XRD report and proves that the MgO/ZnO nanocomposite derived after different temperatures is in pure form.

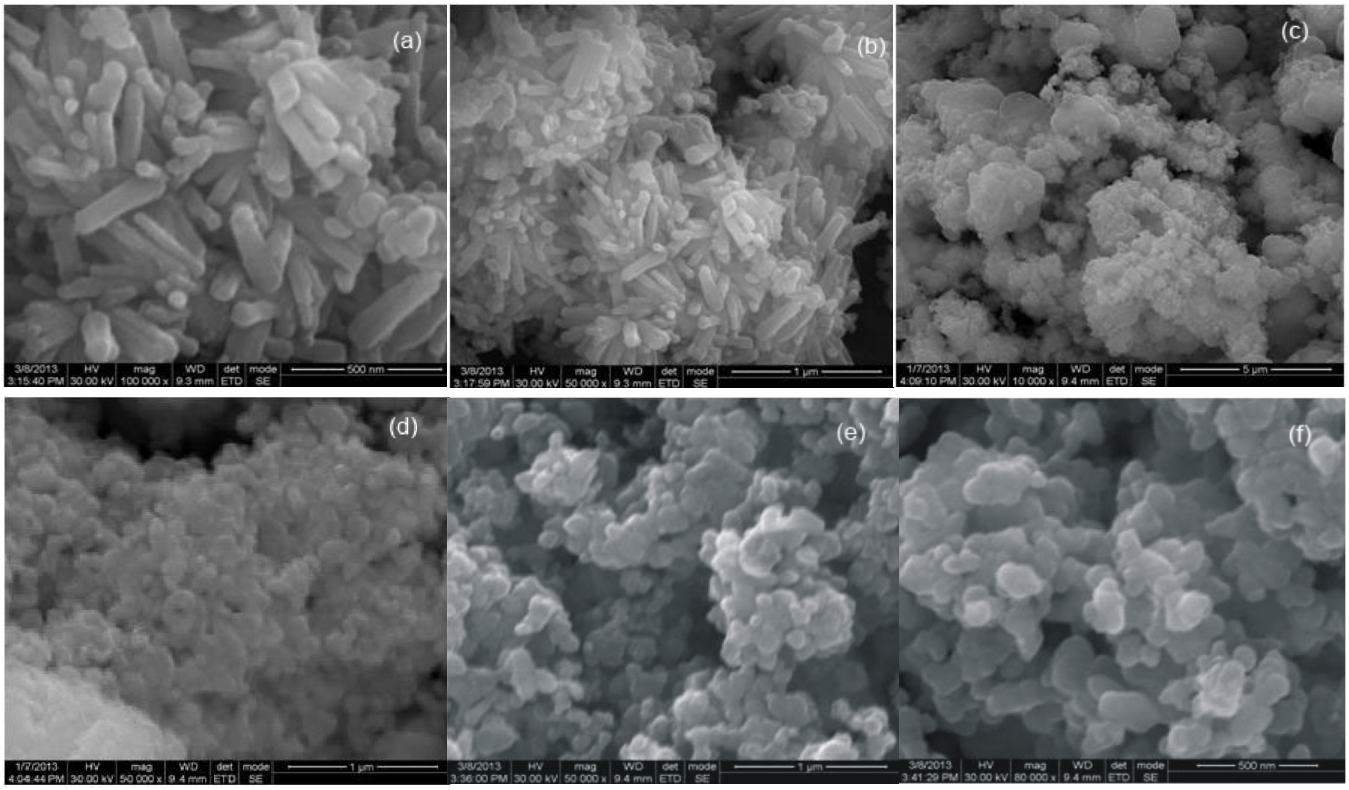

Fig. 4. HRSEM images of (a, b) sample-1, (c, d) sample-2, (e, f) sample-3

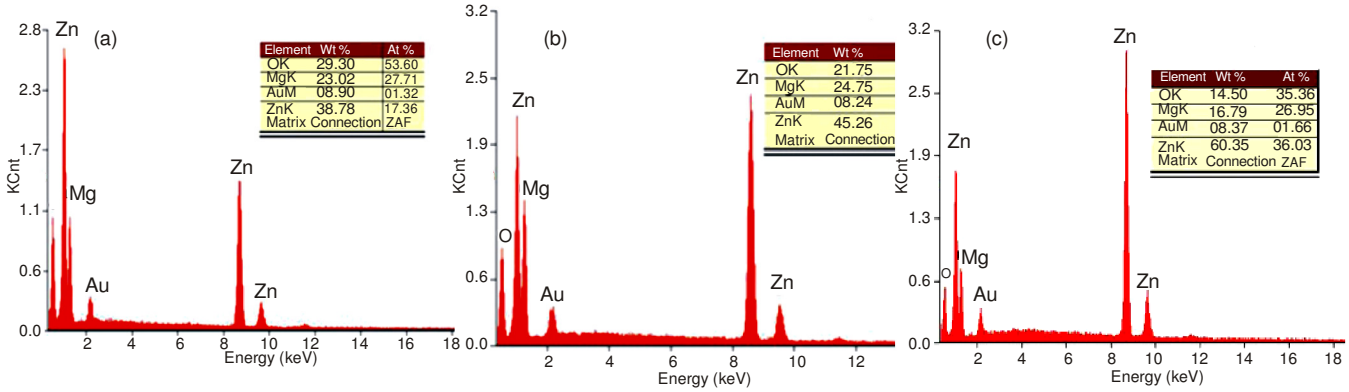

Fig. 5. (a) EDX spectra of MgO-ZnO nanorods (calcining at 400 °C), (b) EDX spectra of MgO-ZnO nanoparticles (calcining at 500 °C) and 5c EDX spectrum of MgO-ZnO nanoparticles (calcining at 600 °C)

UV-visible spectra: The optical absorption spectrum of MgO/ZnO nanocomposite was recorded in the wavelength region of 200-800 nm is shown in Fig. 6. The UV absorption edge of the MgO/ZnO nanocomposite is observed to around 403, 399, 388.73 nm for samples 1, 2, 3, respectively.

The band gap energy is calculated using the Tauc relation. According to the Tauc relation, the absorption coefficient (a) for direct band gap material is given by,

$$\alpha = A(h\nu - E_g)^n / h\nu \quad (2)$$

where E_g is optical band gap of the nanocomposite, A is a constant, hν is the energy of photon and n is an index which assumes the values of 1/2, 3/2, 2 and 3 depending on the nature of electronic transition responsible for reflections. From the Tauc plot of $(\alpha h\nu)^2$ *vs*. hν shown in Fig. 7 band gap energy E_g is evaluated by the extrapolation of the linear part to the X-axis[26] which is found to be 3.07, 3.105 and 3.1898 ev, respectively. This value is found to be less than the already reported values of MgO/ZnO nanocomposites[27]. The band gap calculated from the Tauc plot and UV-visible spectrum is tabulated in Table-2. The less band gap of 3.07 eV is observed for sample-1.

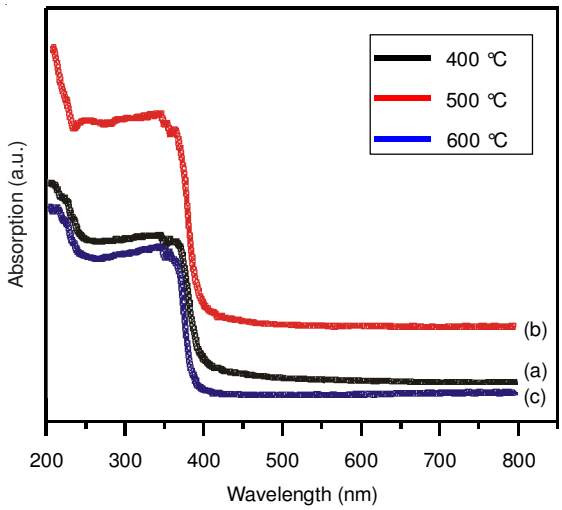

Fig. 6. UV-visible Absorption spectrum of (a) sample-1 (b) sample-2 (c) sample-3

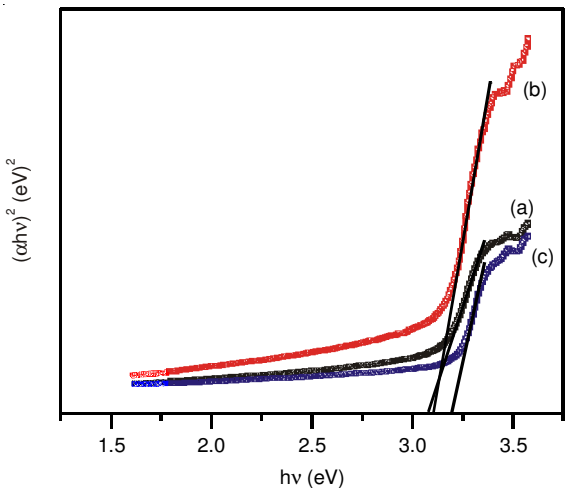

Fig. 7. Tauc plot for (a) sample-1 (b) sample-2 and (c) sample-3

TABLE-2
VARIATION OF BAND GAP AND MORPHOLOGY OF MgO/ZnO NANOPARTICLE

S. No.	Sample	Band gap from UV-visible spectra (eV)	Band gap from Tauc plot (eV)	Morphology
1.	Sample-1	3.077	3.07	Nanorod
2.	Sample-2	3.1054	3.1054	Nanoparticles
3.	Sample-3	3.1869	3.1898	Nanoparticles

Photoluminescence spectra analysis: Fig. 8 shows the photoluminescence spectra of MgO/ZnO nanocomposites synthesized by three different temperatures. In this spectrum all the plots contains two peaks centered at 335 and 396 nm. The sharp UV emission peak at 335 nm is due to band-to-band transition of charge carriers. The other peak centered on 396 nm is originated from exciton recombination corresponding to near band emission (NBE), while the weak signal at 470 nm relates to the transition between the electron close to the conduction band and the hole at vacancy associated with the defects such as, oxygen vacancies, interstitials or impurities[27-30]. The defects are responsible for UV light absorption in ZnO/MgO nanocomposites[31]. Fig. 8 showed that the intensity of PL3 (sample-3) is larger than the peaks of other samples. At 600 °C the morphology of MgO/ZnO nanocomposites is completely spherical. This means that visible emission of spherical shaped MgO/ZnO nanocomposite is larger than rod shaped nanocomposites (formed after the calcination of 400 °C).

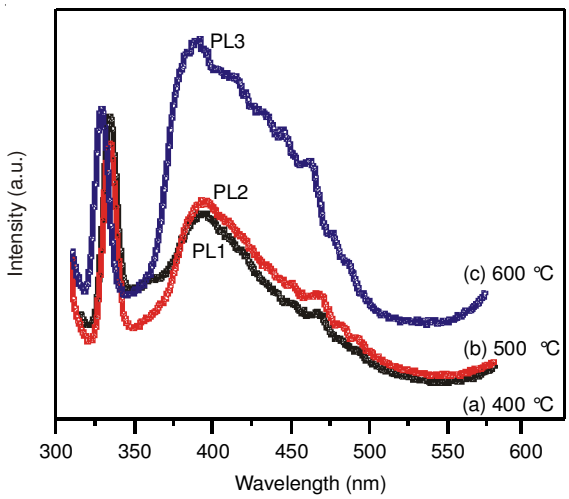

Fig. 8. Photoluminescence spectrum for (a) sample-1 (b) sample-2 and (c) sample-3

Conclusion

MgO/ZnO nanocomposite is successfully synthesized by reflux method. Williamson-Hall plot showed that the micro strain is less for sample annealed at 500 °C. XRD and EDX analysis of the sample annealed at 400, 500 and 600 °C confirms the presence of both cubic MgO and wurtzite ZnO phase. HR-SEM picture reveals that the morphology is strongly influenced by the annealing temperature. At 400 °C, the rod-shaped MgO/ZnO nanocomposite is formed and the complete spherical shape is formed at 600 °C. The band gap is determined by using UV-visible absorption spectra and Tauc plot. The results

obtained by these two methods are nearly same and the band gaps obtained by this method are less compared to the already reported values. The emission peak recorded at 396 and 470 nm from photoluminescence spectrum revealed that the new energy levels were induced by defects.

ACKNOWLEDGEMENTS

The authors expressed their thanks to SAIF, IIT Madras, India for UV-visible, photoluminescence and HRSEM facilities provided.

REFERENCES

1. H. Gao, W. Cai, P. Shimpi, H.-J. Lin and P.-X. Gao, *J. Phys. D Appl. Phys.*, **43**, 272002 (2010).
2. R. Kurahatti, A. Surendranathan, S. Kori, N. Singh, A. Kumar and S. Srivastava, *Def. Sci. J.*, **60**, 551 (2010).
3. Q.G. Al-Zaidi, A.M. Suhail and W.R. Al-Azawi, *Applied Phys. Res.*, **3**, 89 (2011).
4. L.I. Trakhtenberg, G.N. Gerasimov, V.F. Gromov, T.V. Belysheva and O.J. Ilegbusi, *J. Mater. Sci. Res.*, **1**, 56 (2012).
5. N. Yasui, H. Nomura and A. Ide-Ektessabi, *Thin Solid Films*, **447-448**, 377 (2004).
6. Y. Zhao and G. Zhu, *Mater. Sci. Eng. B*, **142**, 93 (2007).
7. I. Sharma, Ambika and P.B. Barman, *Asian J. Chem.*, **21**, S076 (2009).
8. S. Thakoor, H.G. Leduce, J.A. Stern, A.P. Thakoor and S.K. Khanna, *J. Vac. Sci. Technol. Vacuum, Surfaces and Films*, **5**, 1721 (1987).
9. K.M. Lang, D.A. Hite, R.W. Simmonds, R. McDermott, D.P. Pappas and J.M. Martinis, *Rev. Sci. Instrum.*, **75**, 2726 (2004).
10. F. Houze, R. Meyer, O. Schneegans and L. Boyer, *Appl. Phys. Lett.*, **69**, 1975 (1996).
11. H. Kim, C.M. Gilmore, J.S. Horwitz, A. Piqué, H. Murata, G.P. Kushto, R. Schlaf, Z.H. Kafafi and D.B. Chrisey, *Appl. Phys. Lett.*, **76**, 259 (2000).
12. A.P. Chatterjee, P. Mitra and A.K. Mukhopadhyay, *J. Mater. Sci.*, **34**, 4225 (1999).
13. S. Basu and A. Dutta, *Sens. Actuators B*, **22**, 83 (1994).
14. Y. Chen, D. Bagnall and T. Yao, *Mater. Sci. Eng. B*, **75**, 190 (2000).
15. J.G. Ma, Y.C. Liu and C.L. Shao, J.Y. Zhang, Y.M. Lu, D.Z. Shen and X.W. Fan, *Phys. Rev. B*, **71**, 125430 (2005).
16. T. MakinoY. SegawaM. KawasakiA. OhtomoR. ShirokiK. TamuraT. YasudaH. Koinuma. T. Makino, Y. Segawa, M. Kawasaki, A. Ohtomo, R. Shiroki, K. Tamura, T. Yasuda and H. Koinuma, *Appl. Phys. Lett.*, **78**, 1237 (2001).
17. M.A. Karimi, S.H. Roozbahani, R. Asadiniya, A. Hatefi-Mehrjardi, M.H. Mashhadizadeh, R. Behjatmanesh-Ardakani, M. Mazloum-Ardakani, H. Kargar and S.M. Zebarjad, *Int. Nano Lett.*, **1**, 43 (2011).
18. M. Gao, J.H. Yang, L.L. Yang, Y.J. Zhang, H.L. Liu, H.G. Fan, J.H. Lang, Y.R. Sui, B. Feng, Y.F. Sun, Z.Q. Zhang and H. Song, *Appl. Phys. B*, **112**, 539 (2013).
19. S. Chitanya Lakshmi, Ananda, R. Somashekar and C. Ranganathaiah, *Int. J. Nanosci. Nanotechnol.*, **3**, 47 (2012)..
20. D. Ramimoghadam, M. Bin Hussein and Y. Taufiq-Yap, *Chem. Cent. J.*, **7**, 136 (2013).
21. S. Talam, S.R. Karumuri and N. Gunnam, *ISRN Nanotechnology*, Article ID 372505 (2012).
22. Y. Ding, G. Zhang, H. Wu, B. Hai, L. Wang and Y. Qian, *Chem. Mater.*, **13**, 435 (2001).
23. M. Pashchanka, R.C. Hoffmann and J.J. Schneider, *J. Mater. Chem.*, **20**, 957 (2010).
24. B. Cao and W. Cai, *J. Phys. Chem. C*, **112**, 680 (2008).
25. V.D. Mote, Y. Purushotham and B.N. Dole, *J. Theoret. Appl. Phys.*, **6**, 6 (2012).
26. G.N.S. Vijayakumar, S. Devashankar, M. Rathnakumari and P. Sureshkumar, *J. Alloys Comp.*, **507**, 225 (2010).
27. S. Chawla, K. Jayanthi, H. Chander, D. Haranath, S.K. Halder and M. Kar, *J. Alloys Comp.*, **459**, 457 (2008).
28. D. Banerjee, J.Y. Lao, D.Z. Wang, J.Y. Huang, D. Steeves, B. Kimball and Z.F. Ren, *Nanotechnology*, **15**, 404 (2004).
29. W.-C. Sun, Y.-C. Yeh, C.-T. Ko, H. He and M.-J. Chen, *Nanoscale Res. Lett.*, **6**, 556 (2011).
30. X. Qiu, G. Li and L. Li, *J. Mater. Res.*, **22**, 908 (2007).
31. S.K. Chaudhuri, M. Ghosh, D. Das and A.K. Raychaudhuri, *J. Appl. Phys.*, **108**, 064319 (2010).